Visualizing the Aftermath of Volcanic Eruptions

Tobias Günther
University of Magdeburg

Maik Schulze
University of Magdeburg

Anke Friederici
University of Magdeburg

Holger Theisel
University of Magdeburg

ABSTRACT

Volcanic eruptions are not only hazardous in the vicinity of a volcano, but also affect the climate and air travel at larger distance. In this paper, we present our results on the 2014 IEEE Scientific Visualization Contest, which centers around the fusion of multiple satellite data modalities to reconstruct and assess the movement of ash clouds. In particular, we shed light on the Grímsvötn, Puyehue-Cordón Caulle and Nabro eruptions in 2011. We study the agreement of the satellite data, reconstruct the ash clouds, visualize endangered flight routes, minimize occlusion of particle trajectories and finally focus on the pathways of aerosol into the stratosphere.

1 INTRODUCTION

In this paper, we present our findings on the aftermath of three volcanic eruptions as a contribution to the 2014 IEEE Scientific Visualization Contest. Our analysis is based on the fusion of different climate data modalities in order to assess the plume development of volcanic ash and sulfate aerosol emitted from the volcanoes Grímsvötn in Iceland (eruption at May 21st, 2011), Puyehue-Cordón Caulle in Chile (eruption at June 4th, 2011) and Nabro in Eritrea (eruption at June 13th, 2011).

The contest data comprises discrete, time-dependent, vertical ash and sulfate aerosol detections by the Michelson Interferometer for Passive Atmospheric Sounding (MIPAS) [3], which produced roughly 1.29 million points (42 MB of memory in total). Furthermore, ash and SO_2 indices are measured on thin polygon strips by the Atmospheric Infrared Sounder (AIRS) [1], which results in 12.8 GB of memory for the entire time sequence. Trajectories of 61,324 particles are seeded at MIPAS detections and are simulated by the Chemical Lagrangian Model of the Stratosphere (CLaMS) [6]. The trajectories and their associated scalars, e.g., temperature and pressure, sum up to 1.04 GB. The simulation is based on ERA-Interim [2] data; same as the tropopause altitude measurements. The tropopause altitudes (potentially two layers) are provided on a uniform grid for 320 time steps, which totals in 477 MB. The principal data setup is illustrated in Fig 1.

2 DATA PREPROCESSING

Determined by the satellite trajectories, the MIPAS and AIRS measurements are arranged along roughly sinusoidal ground tracks that cover the globe, see again Fig. 1. Since both satellites orbit the globe about 14 times a day and measure only within a small band, the concentration indices and detection measurements are quite sparsely represented in both space and time. To fill in the blank areas in AIRS, we interpolate values from the two closest time steps and inspect the temporal distance in Fig. 2. As shown, this interpolation method entails small reconstruction artifacts. To suppress noise, the interpolated measurements are convolved with a Gaussian kernel. For faster access on the GPU, we resample the AIRS data onto a uniform grid with 1000×500 cells at 600 time steps, which totals for both ash and SO_2 indices in 2×1.11 GB.

3 DATA ANALYSIS

The data is within gigascale range, making it comfortable to process it on a single machine. Thus, we keep all AIRS, MIPAS, CLaMS and the tropopause data in RAM and selectively stream the data of the current time slice to the GPU for display. First, we integrate the data into a comprehensive and interactive overview visualization, as described in the following.

3.1 Overview and Data Browsing

An overview of the data is shown in Fig. 3. Here, all MIPAS, AIRS and CLaMS can be interactively explored, transfer functions adjusted and data attributes visualized, such as altitude, pressure or temperature. Combining individual satellite data into one visualization also allows to locate and judge areas at which the modalities disagree. In Fig. 4, we map at each MIPAS ash and sulfate aerosol detection the corresponding AIRS concentration indices to color. In addition, we create histograms of AIRS indices sampled at MIPAS detections. It is apparent that especially the MIPAS sulfate aerosol detections are very sensitive and placed in areas of no particularly increased AIRS measurements.

3.2 Linking the Measurements to the Volcanoes

The volcanic eruptions happened in a span of three weeks. While Puyehue-Cordón Caulle seems easily separable from the others as it is on the Southern Hemisphere, Grímsvötn and Nabro are close enough for their aerosol clouds to mix. As it turns out, there are some trajectories on the Northern Hemisphere that originated near Puyehue-Cordón Caulle in the South. Thus, due to the intermixing of particles across the entire globe, a mere thresholding by the latitude is not optimal to isolate Puyehue-Cordón Caulle. In order to identify the volcano that emitted the ash or sulfate aerosol that was found by a particular MIPAS detection, we trace the CLaMS trajectories backward in time. For each vertex of a trajectory, we compute the distance to all volcanoes and consider the closest a potential source, if the volcano was passed while it was active. From there on, a CLaMS trajectory and potentially its MIPAS detection (the seed point) are associated with the closest volcano if the minimal distance is below a user-defined threshold, which we empirically set to about 250 km. Since the CLaMS trajectories in the North start at the time of the Nabro eruption, they cannot be used to determine whether a MIPAS detection belonged to the earlier Grímsvötn eruption. Eventually, we end up with a number of MIPAS aerosol detections (80.5 %) that cannot be associated with a volcano. Using the AIRS measurements, we identify further MIPAS and CLaMS detections by using a suitable threshold on the ash index. (We found the sulfate aerosol concentrations to be insufficiently descriptive.) The histogram in Fig. 4 suggests that MIPAS detects ash in regions with an ash index < 4, which we use as a conservative threshold. Later, transparency is used to fade out areas with an ash index > 0, but during cloud reconstruction it is advisable to have more trajectories that carry potentially varying ash concentrations. If these ash detections are north of 55° N and not yet associated with a volcano they are likely to belong to Grímsvötn, which equals to roughly 1.0 % of all MIPAS ash or sulfate aerosol detections. A classification of the CLaMS trajectories to the potential source volcanoes is shown in Fig. 5.

3.3 Ash Cloud Reconstruction

We move on to the reconstruction of the ash clouds, which we discretize into a uniform 3D scalar field with $1000 \times 500 \times 32$ voxels. AIRS measurements are altitude-integrated, which we distribute along the altitude using CLaMS and MIPAS. For this, we create at every AIRS measurement a probability distribution $f(z)$ of the ash concentration along the altitude z. Thereby, we aim for two things. First, MIPAS detections should be transported along CLaMS trajectories, as these are the actual pathways of the ash. Second, $f(x)$ should correspond to CLaMS density, as more lines are likely to transport more ash. For the first, we start at the MIPAS seed vertices and follow the trajectories in both directions. In case a MIPAS detection is located nearby (in a range of 128 km, at an altitude difference of less than 5 km and a time difference of less than 1.5 hours) we assign from there on the detection on the line (e.g., air $= 0$ or ash $= 1$). Afterwards, we diffuse it, assuming that the detected ash is transported. For the second, we rasterize the detection values of all CLaMS trajectories into a 3D scalar field, using additive blending. We use one scalar field for each volcano and another one for unclassified trajectories in order to discriminate them. Thereby, we obtain an ash detection frequency h_v at every voxel v. To ensure independence of the grid resolution, the ash concentration $c(z)$ of a voxel is obtained by dividing h_v by the voxel volume. The probability distribution $f(z)$ of the ash concentration follows from normalizing the ash concentration $c(z)$ such that $\int f(z)\mathrm{d}z = 1$. Using the 2D AIRS ash index $A_{2\mathrm{D}}$, we reconstruct our 3D ash index $A_{3\mathrm{D}}(z)$ as:

$$A_{3\mathrm{D}}(z) = A_{2\mathrm{D}}\, f(z) - \gamma c(z)\,.$$

Setting $\gamma = 0$ distributes the AIRS ash index along the altitude axis according to the probability distribution $f(z)$, thereby trusting only AIRS. But since MIPAS is known to be more sensitive than AIRS, we introduce a γ-parameter that allows the MIPAS-guided ash concentration $c(z)$ to overrule the AIRS decision. In its essence, γ balances the trust between AIRS and MIPAS. Reconstructed ash clouds are shown in the next section. Following the same idea, sulfate aerosol clouds are visualized in Fig. 6 by GPU-based ray casting. The clouds are shaded by Fourier opacity mapping [5].

3.4 Dangerous Flight Routes

Using OpenFlights air traffic data, we generate 73,098 examplary airplane routes, which are visualized in Fig. 7. Based on the reconstruction of the ash clouds, we extract flight routes that pass a region with a negative ash index $A_{3\mathrm{D}} < 0$. The animation in the accompanying video shows when airports in Chile, Argentina, South Africa, Southern Australia and New Zealand were worst affected by the Puyehue-Cordón Caulle ash cloud.

3.5 Visualization of CLaMS Trajectories

The CLaMS trajectories are essential for the linking of MIPAS measurements to the volcanic events. Their sheer number, however, makes it difficult to visualize them properly, because of occlusions. Thus, in Fig. 8, we use hierarchical opacity optimization [4], a recent visualization method that adjusts the opacity of lines in order to minimize the occlusion of important—here, sulfate aerosol-laden—lines. Thereby, we not only obtain a notion of the location of sulfate aerosol clouds, but also see transport paths as context. In Fig. 9, we show a 3D close-up on CLaMS trajectories that are associated with the Nabro volcano. The lines near the ground visualize the path of sulfate aerosol that is carried within the Asian Monsoon circulation, which lifts up near the East China Sea. Above, far more trajectories are shown that entered the stratosphere elsewhere, which is discussed next.

3.6 Aerosol in the Stratosphere

When aerosol enters the stratosphere it remains there for months or years, where it absorbs solar radiation, leading to a cooling of the surface. At present, there is an ongoing dispute among climate scientists on how Nabro's aerosol entered the stratosphere. Two hypotheses exist that argue for a direct injection at the volcanic emission (H1) or the upward motion within the Asian Monsoon circulation (H2). The CLaMS trajectories that are relevant for the support or decline of these hypotheses and their intersections with the tropopause layer are shown in Fig. 10. The correlation of the scalar CLaMS attributes (potential temperature/vorticity, pressure, temperature) with the tropopause intersection is visualized in Fig. 11. The visualization suggests that there are not only two but *three* possible pathways into the stratosphere. All but the potential vorticity criterion show fairly good agreement on that. The direct injection (H1) takes place at the volcano in Eritrea and in the western downwind. The Asian Monsoon circulation (H2) transports fewer particles eastward, which uplift near the East China Sea, as shown in Fig. 9(b). Most of the aerosol is carried westwards, taking a north-east turn above the Sahara. Then, another large part of the aerosol seems to enter the stratosphere above Northern India and Nepal (H3). The frequency of the events suggests that (H1) and (H3) are likewise the main pathways into the stratosphere. The Summer Monsoon circulation (H2) has a smaller, yet measurable contribution.

4 Implementation

Our test system is equipped with an Intel Core i7-2600K CPU with 3.4 GHz, 24 GB RAM and an Nvidia GeForce GTX 560 Ti GPU with 2 GB VRAM. The rendering resolution is at 1440×720 pixels with $4\times$MSAA. During preprocessing, the resampling of the AIRS data took 36 minutes and the mapping of MIPAS detections onto the CLaMS trajectories took 2.3 minutes. At runtime, the visualization reaches interactive frame rates. For instance, the illustrations in Fig. 11 are rendered at 67 frames per second. The rendering of the clouds in Fig. 6 is done at 14 frames per second. The extraction of the cloud scalar fields takes 300 ms and is only performed when a parameter changes.

The visualizations are created in a specifically tailored C++ program that uses Direct3D 11 for rendering. In addition, we used standard tools such as ParaView and ZIB Amira for display of intermediate results throughout the development.

References

[1] M. T. Chahine, T. S. Pagano, H. H. Aumann, R. Atlas, C. Barnet, J. Blaisdell, L. Chen, M. Divakarla, and et al. AIRS: Improving weather forecasting and providing new data on greenhouse gases. *Bulletin of the American Meteorological Society*, 87(7):911–926, 2006.

[2] D. P. Dee, S. M. Uppala, A. J. Simmons, P. Berrisford, P. Poli, S. Kobayashi, U. Andrae, and et al. The ERA-interim reanalysis: configuration and performance of the data assimilation system. *Quarterly Journal of the Royal Meteorological Society*, 137(656):553–597, 2011.

[3] S. Griessbach, L. Hoffmann, R. Spang, and M. Riese. Volcanic ash detection with infrared limb sounding: MIPAS observations and radiative transfer simulations. *Atmospheric Measurement Techniques*, 7(5):1487–1507, 2014.

[4] T. Günther, C. Rössl, and H. Theisel. Hierarchical opacity optimization for sets of 3D line fields. *Computer Graphics Forum (Proc. Eurographics)*, 33(2):507–516, 2014.

[5] J. Jansen and L. Bavoil. Fourier opacity mapping. In *Proc. Symposium on Interactive 3D Graphics and Games*, pages 165–172, 2010.

[6] P. Konopka, H.-M. Steinhorst, J.-U. Groo, G. Günther, R. Müller, J. W. Elkins, H.-J. Jost, E. Richard, U. Schmidt, G. Toon, and D. S. McKenna. Mixing and ozone loss in the 1999–2000 arctic vortex: Simulations with the three-dimensional chemical lagrangian model of the stratosphere (CLaMS). *Journal of Geophysical Research: Atmospheres*, 109(D2), 2004.

[7] M. Zöckler, D. Stalling, and H.-C. Hege. Interactive visualization of 3D vector fields using illuminated stream lines. In *IEEE Visualization*, pages 107–113, 1996.

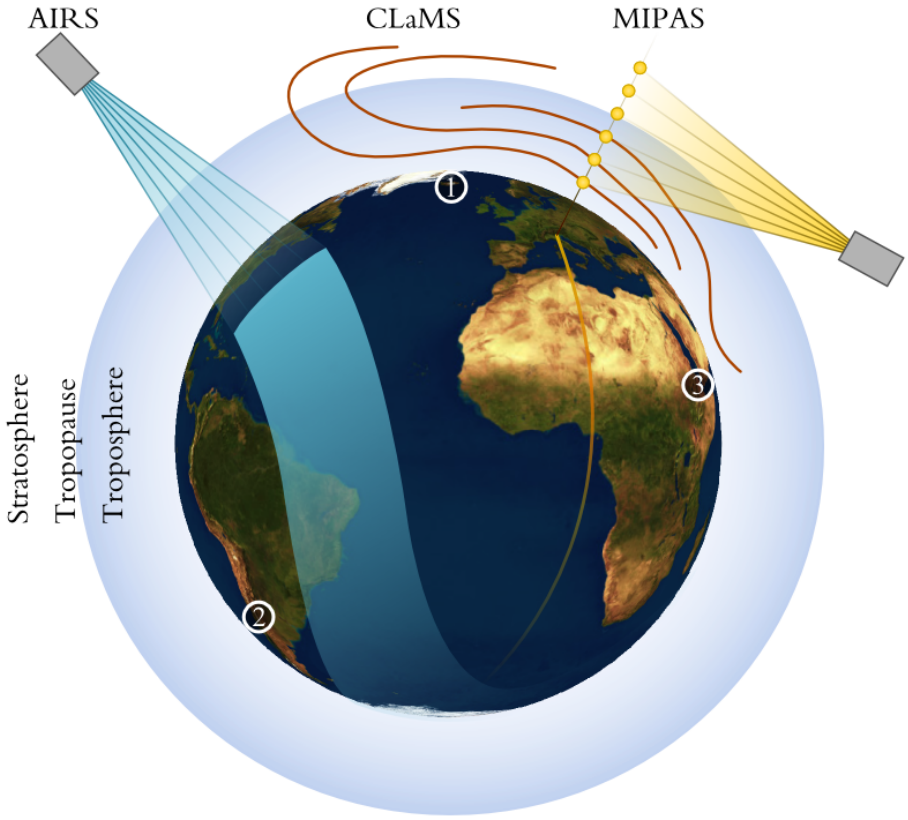

Figure 1: This image gives an overview of the principal data setup. MIPAS detects sulfate aerosol and ash vertically, whereas AIRS uses index methods to measure altitude-integrated SO_2 and ash particle concentration. The measurements are taken along roughly sinusoidal ground tracks, which leaves numerous areas blank. CLaMS trajectories are seeded at MIPAS detections of volcanic ash or sulfate aerosol. The locations of the volcanoes are shown by numbers: (1) Grímsvötn in Iceland (eruption at May 21st, 2011), (2) Puyehue-Cordón Caulle in Chile (eruption at June 4th, 2011) and (3) Nabro in Eritrea (eruption at June 13th, 2011).

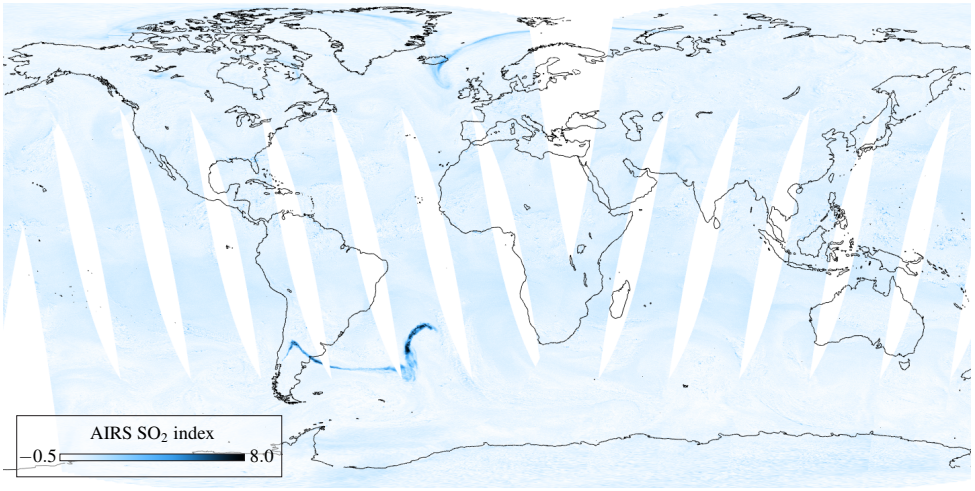

(a) Original AIRS data (12 hours time frame).

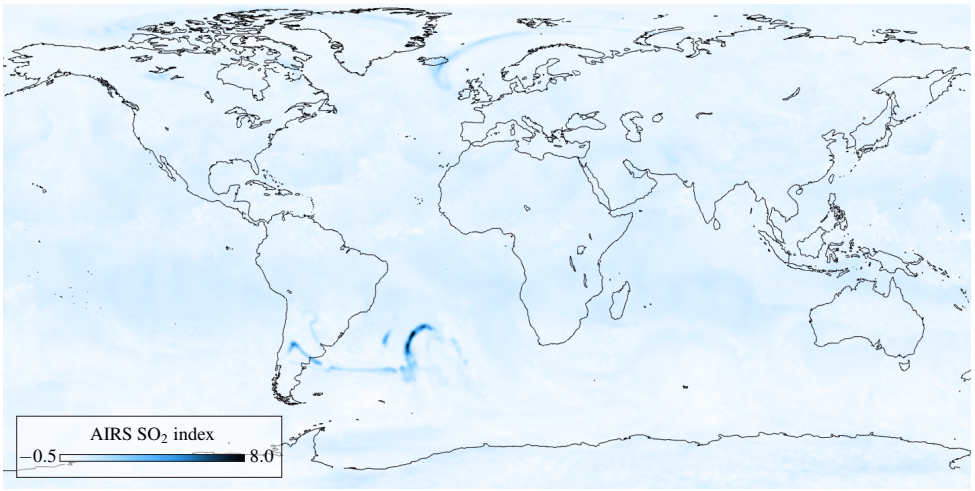

(b) Resampled AIRS data (single time slice).

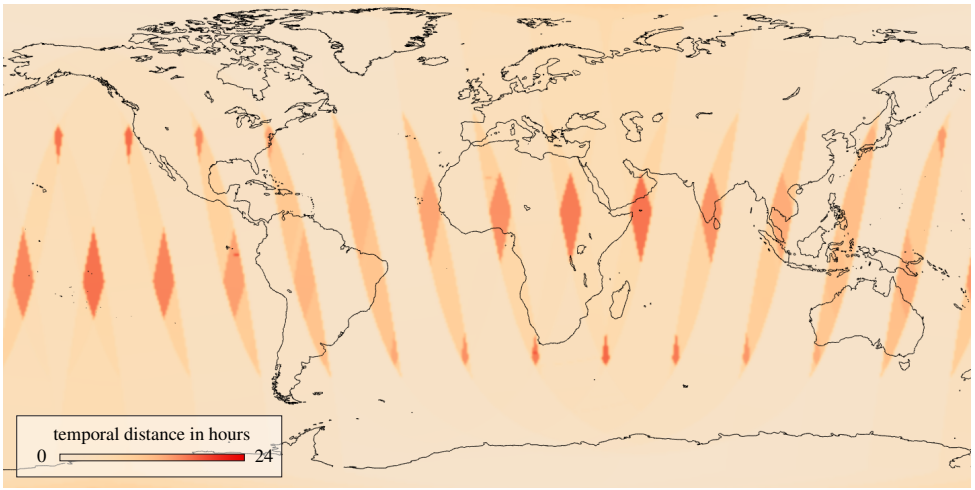

(c) Temporal distance to the closest measurement.

Figure 2: This figure displays preprocessing results of AIRS data. The first two images show the SO_2 index on June 6th, measured shortly after the eruption of the Puyehue-Cordón Caulle volcano. The original data (a) has measurement gaps, which we fill in a resampling step (b). Note that reconstruction artifacts may appear, as we interpolate values from nearby time slices. The temporal distance to the closest measurement is shown in (c).

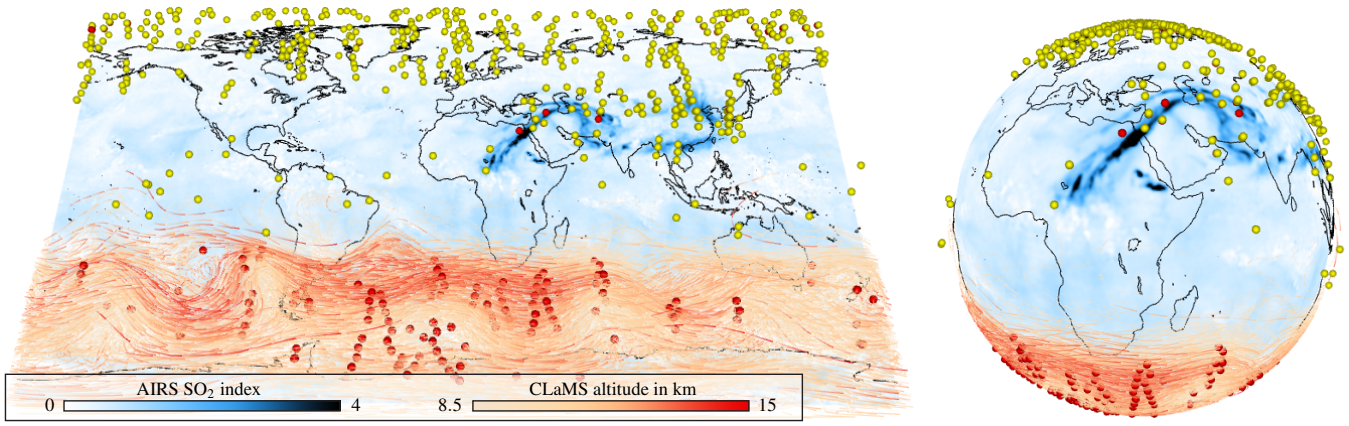

Figure 3: Here, the main input data (MIPAS, AIRS and CLaMS) is combined in an interactive visualization that allows to slice in time, apply transfer functions, and map varying data attributes (pressure, temperature, etc.) to the trajectories. The user can instantly switch between a planar 3D view with altitude mapped to height and a spherical view, which both have individual strenghts and weaknesses, i.e., distortion at the poles and occlusion of the backfacing hemisphere. Currently June 18th is selected, with trajectories shown for a time frame of 3 days. The CLaMS trajectories are only shown for the Southern Hemisphere and are color-coded by altitude. The MIPAS detections are depicted as colored dots, with yellow encoding a sulfate aerosol and red an ash detection. MIPAS detections of air and ice are hidden in this image. The map in the background color-codes resampled AIRS values, showing an SO_2 cloud emitted from the Nabro volcano.

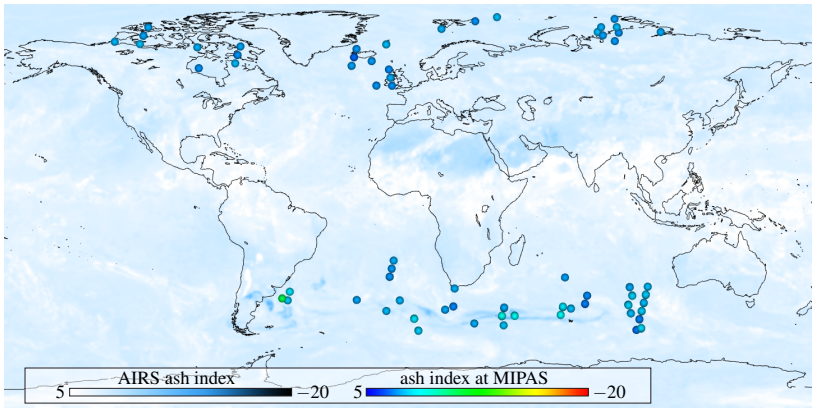

(a) Ash index on June 8th, shortly after the Puyehue-Cordón Caulle eruption.

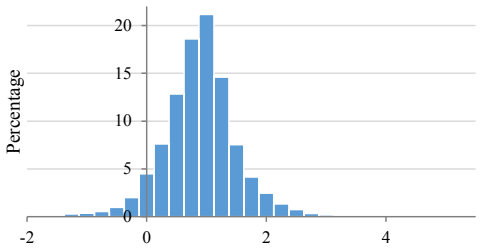

(b) Histogram of sampled AIRS ash indices at MIPAS ash detections.

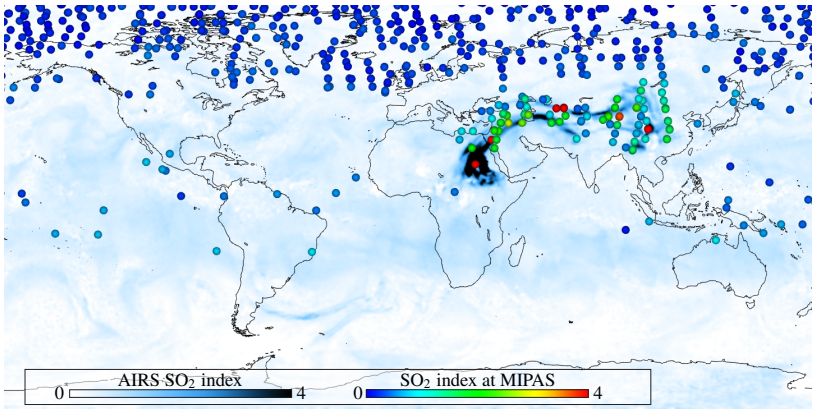

(c) SO_2 index on June 16th, shortly after the Nabro eruption.

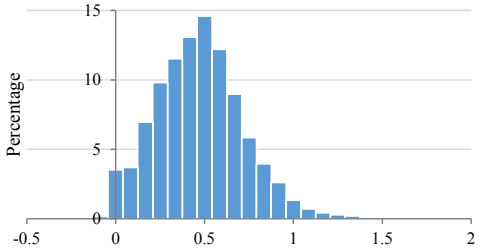

(d) Histogram of sampled AIRS SO_2 indices at MIPAS sulfate aerosol detections.

Figure 4: MIPAS and AIRS exhibit a different sensitivity to aerosols. Consequentially, it is expected that both satellites will reach different answers in areas of low concentration. Figs. (a) and (c) color-code AIRS concentration indices at the MIPAS detections in a time frame of 3 days, centered at June 8th and June 16th, respectively. The ash index histogram in Fig. (b) (of the entire sequence) shows that the majority of the MIPAS detections has an ash index < 4. For sulfate aerosol in Fig. (d), however, many detections are in range of a particularly low AIRS SO_2 index. As visible on the map, most of these detections occur in the North.

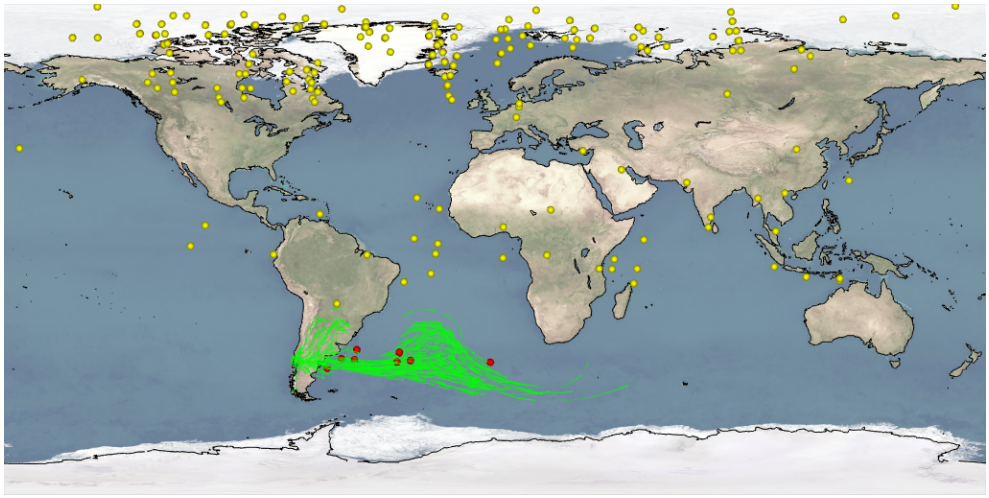

(a) June 6th, two days after Puyehue-Cordón Caulle eruption.

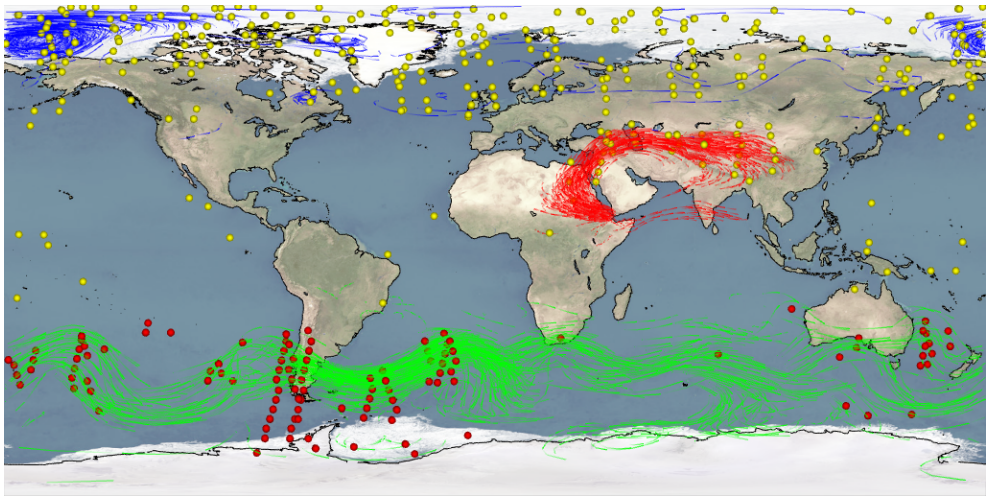

(b) June 16th, three days after Nabro eruption.

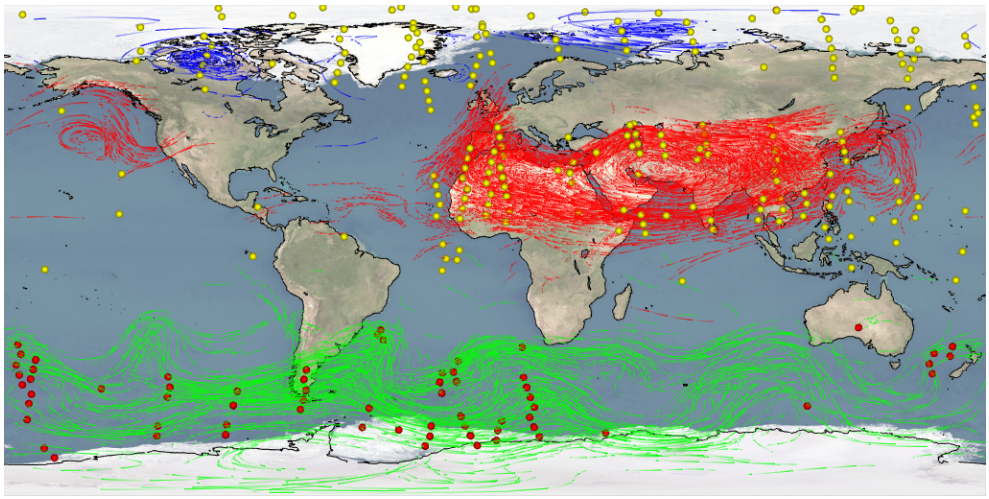

(c) June 28th, fifteen days after Nabro eruption.

Figure 5: In this figure, the classification of CLaMS trajectories to the three volcanoes Grímsvötn (•), Puyehue-Cordón Caulle (•) and Nabro (•) is shown. The three images depict a 36 hours time frame, centered shortly after the eruption of Puyehue-Cordón Caulle (a), the eruption of Nabro (b) and then 12 days later (c). For reference, MIPAS detections are shown by points in yellow (sulfate aerosol) and red (ash).

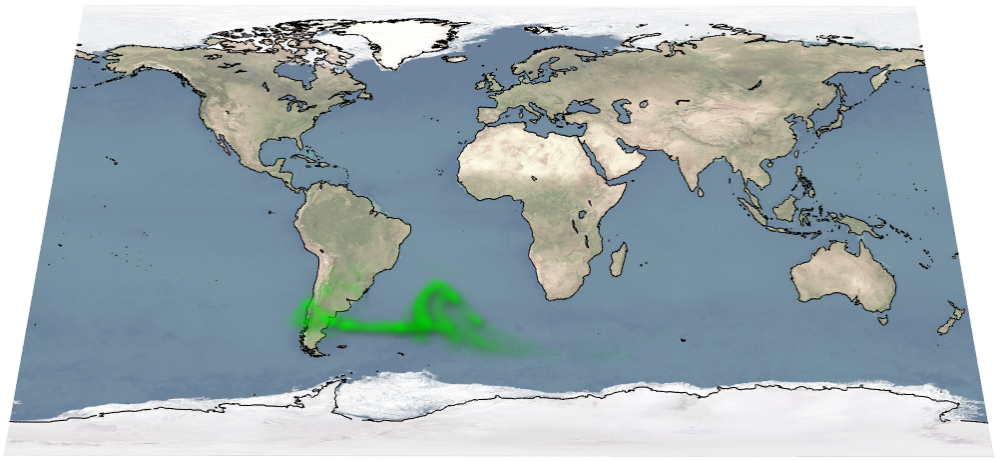

(a) June 6th, two days after Puyehue-Cordón Caulle eruption.

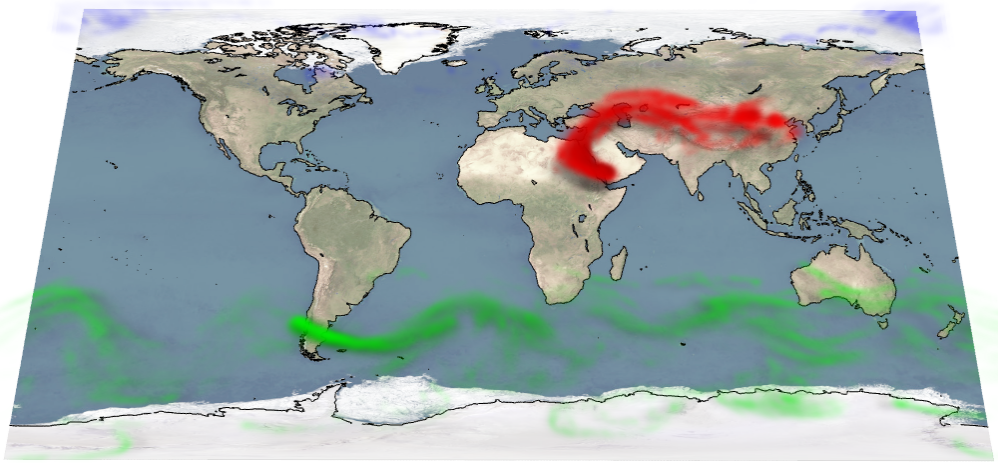

(b) June 16th, three days after Nabro eruption.

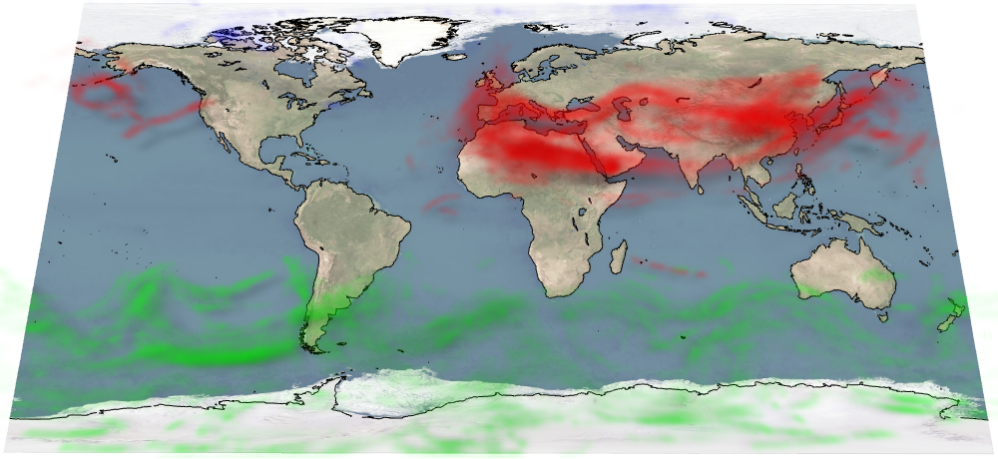

(c) June 28th, fifteen days after Nabro eruption.

Figure 6: This visualization depicts the reconstructed 3D sulfate aerosol clouds. The time frame and line set were the same as in Fig. 5. Similarly, the clouds of the volcanoes Grímsvötn (•), Puyehue-Cordón Caulle (•) and Nabro (•) are color-coded. Note that, while the Grímsvötn eruption starts at May 21st, the CLaMS trajectories on the Northern Hemisphere start no sooner than June 12th. Consequentially, only residuals of the Grímsvötn cloud are reconstructed by our method. On the Northern Hemisphere, CLaMS, MIPAS and AIRS are combined, whereas on the Southern Hemisphere only CLaMS and AIRS could be used, since there are no MIPAS sulfate aerosol detections south of 20° S. We refer to the accompanying video for animations.

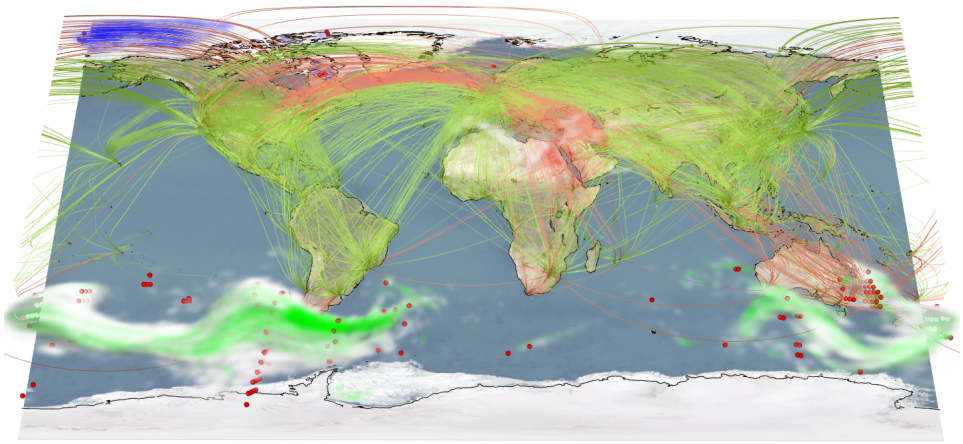

(a) Airplane routes on June 15th.

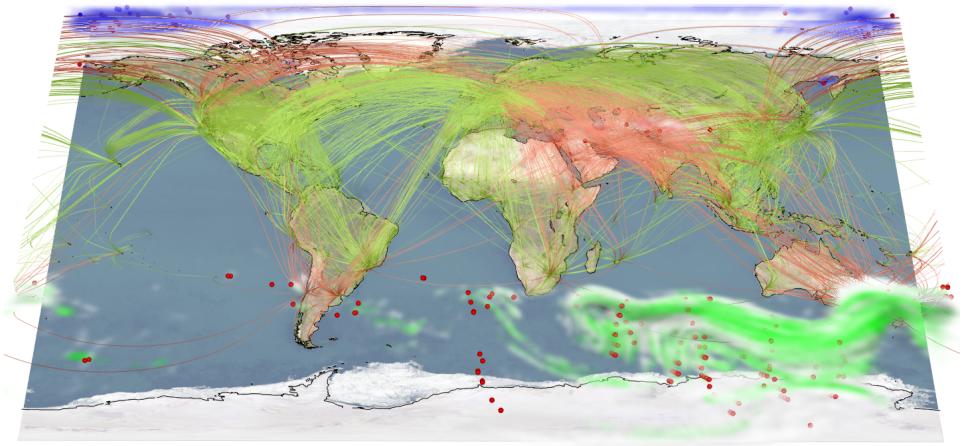

(b) Airplane routes on June 21st.

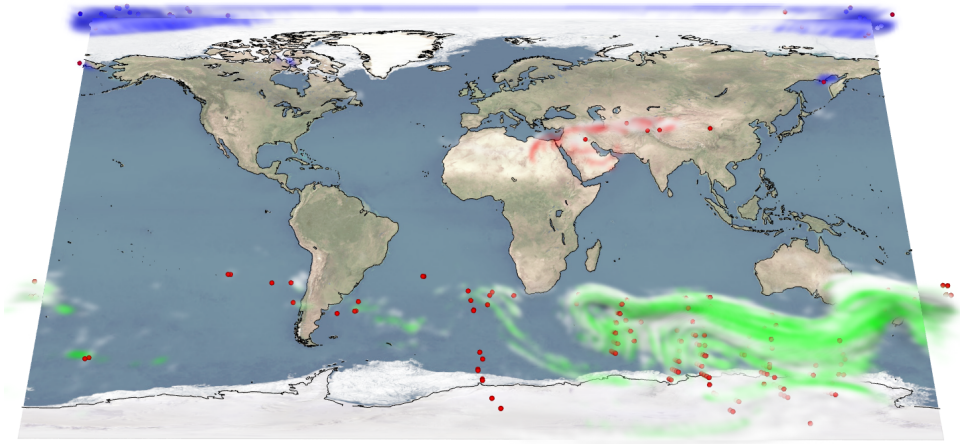

(c) Ash clouds on June 21st with an ash index < 0.

Figure 7: This visualization shows the reconstructed 3D ash clouds for $\gamma = 2$ in a 36 hours time frame. The clouds of the volcanoes Grímsvötn (•), Puyehue-Cordón Caulle (•) and Nabro (•) are color-coded, whereas white clouds denote ash that our heuristic did not associate with a volcano. The MIPAS ash detections are color-coded in red for reference, showing that we are able to reconstruct the clouds at those sensitive detections, which would have not been able with AIRS alone. In (a) and (b) flight routes are intersected with the ash clouds, showing safe airplane routes (green) and routes that should be canceled, as they would enter a dangerous flight corridor (red). In (c) only ash clouds and MIPAS ash detections are shown to allow for a clearer view on the cloud reconstruction results. For comparison, the accompanying video contains the reconstructed ash clouds for $\gamma = 0$, i.e., a 3D ash index solely based on AIRS.

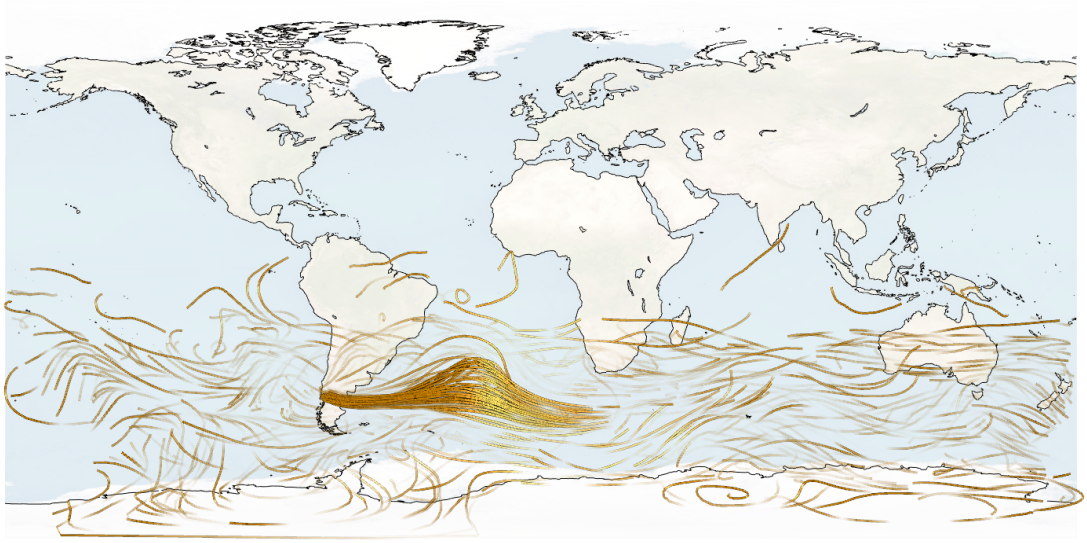

(a) June 4th – June 8th, with opacity optimization.

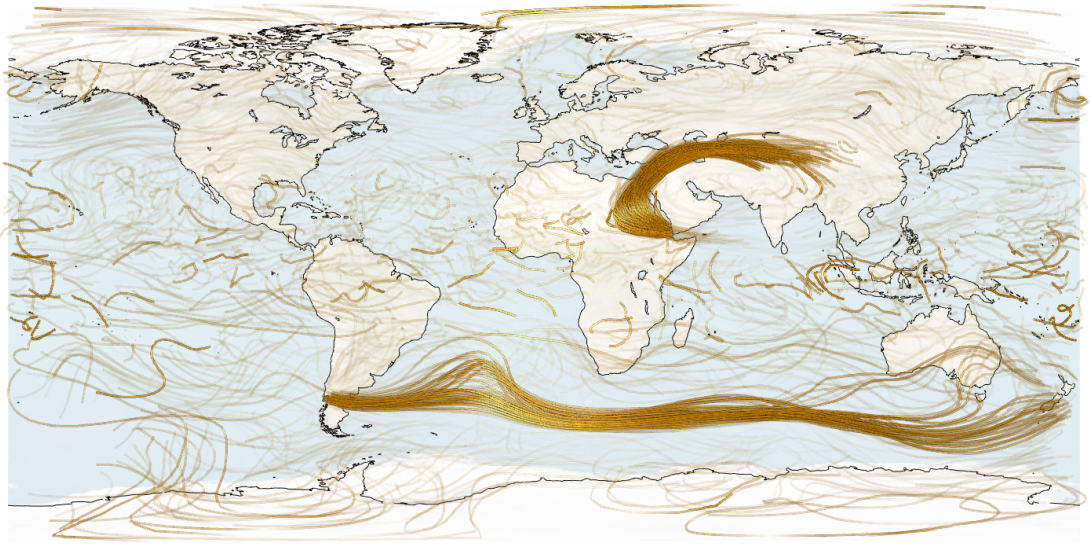

(b) June 4th – June 16th, with opacity optimization.

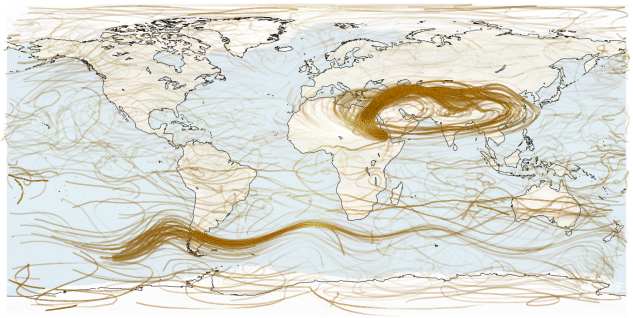

(c) June 13th – June 27th, with opacity optimization.

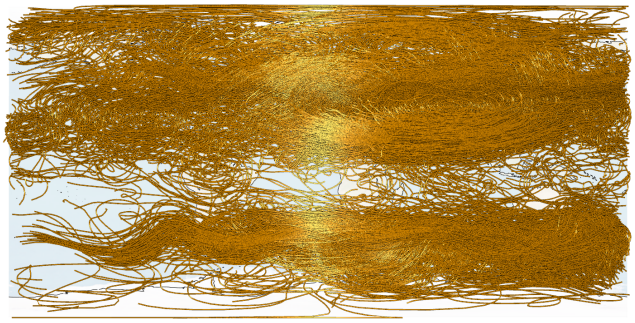

(d) June 13th – June 27th, opaque (input line set).

Figure 8: CLaMS trajectories occlude each other rather strongly. For this reason, we use hierarchical opacity optimization [4], which computes an optimal assignment of line opacities so that the view is cleared on CLaMS trajectories with high sulfate aerosol concentration. Thereby, unclassified trajectories serve as context and fade out if they hide relevant lines. The figures (a)–(c) show CLaMS trajectories in different time frames. Figure (d) shows a highly cluttered line set, which was used as input for the opacity optimization in (c). The lines are shaded as illuminated streamlines [7].

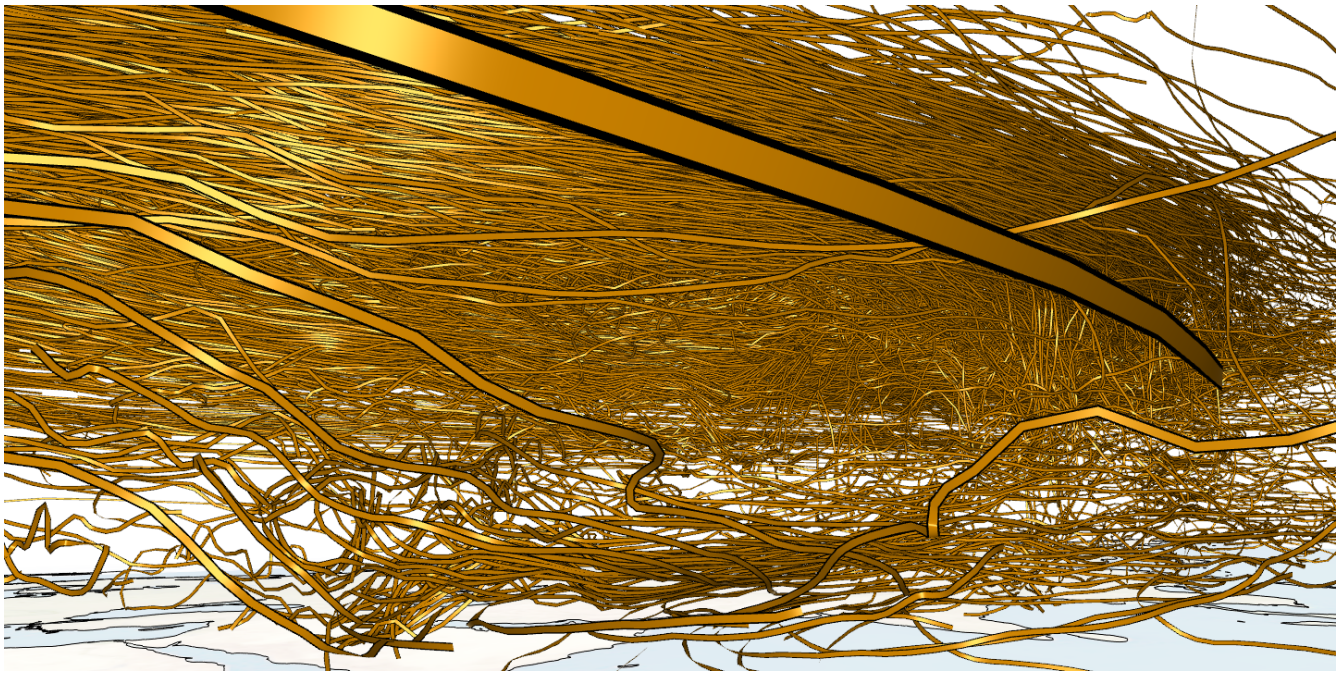

(a) June 21st – July 5th, opaque (input line set).

(b) June 21st – July 5th, with opacity optimization.

Figure 9: Here, hierarchical opacity optimization [4] is used to clear the view on Nabro CLaMS trajectories that have a high aerosol concentration and are affected by the Asian Monsoon circulation. Image (a) contains the cluttered input lines for which opacities are optimized in image (b). For this 3D close-up, the camera is placed above Southern Africa looking north-northeast. Lines that start high above the volcano show aerosol that has been directly injected into the upper tropopause or even into the stratosphere. The altitude of the lines is scaled considerably to make the altitude difference between lines in the stratosphere and in the Asian Monsoon apparent.

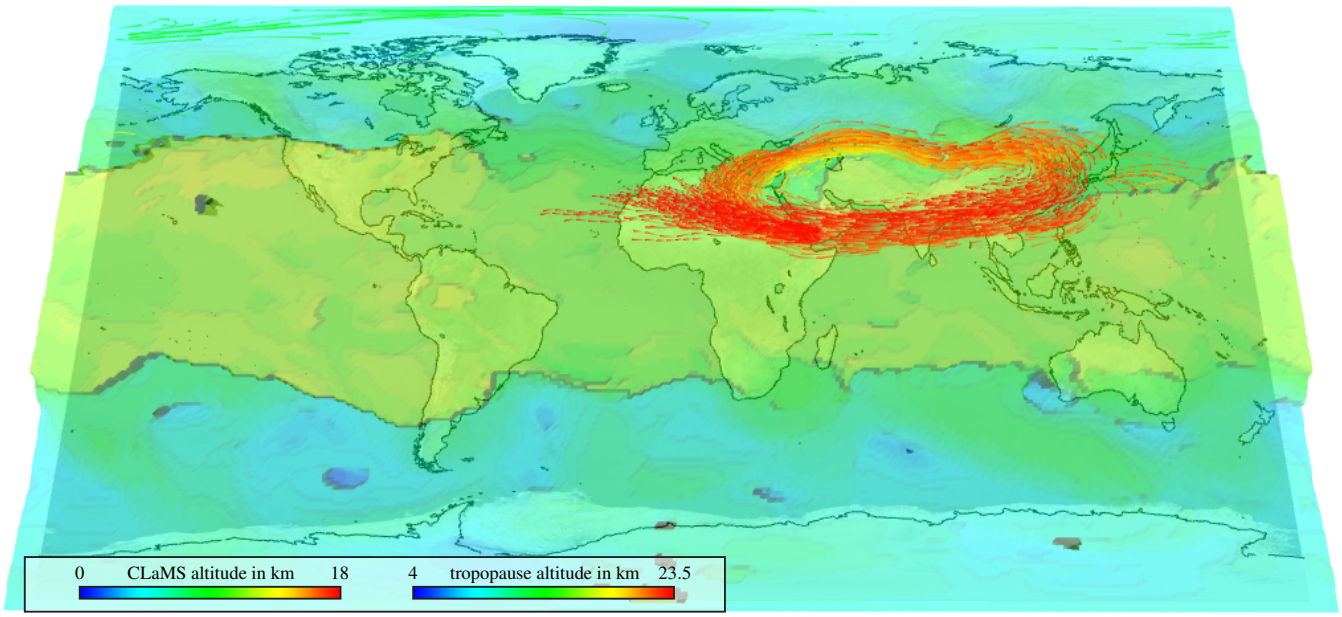

(a) A 3D top view on the lower tropopause geometry layer and the CLaMS trajectories that are associated with the Nabro volcano. In this image only the parts of the CLaMS trajectories are shown that are *above* the lower tropopause, i.e., are stratospheric trajectories. In the stratosphere, trajectories move in a clock-wise circular motion over Northern Africa and Asia.

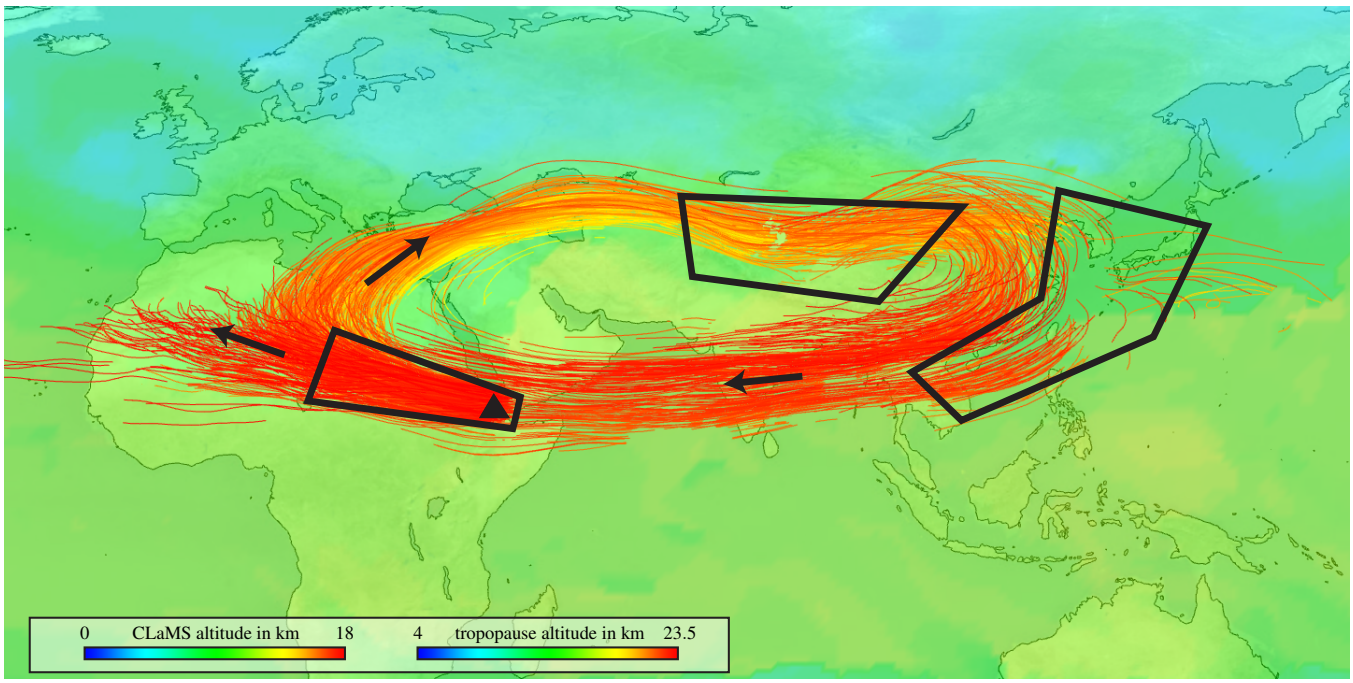

(b) A 2D close-up on stratospheric CLaMS trajectories that are associated with the Nabro volcano reveals areas in which CLaMS trajectories enter the stratosphere: Eritrea, Northern India and the East China Sea.

Figure 10: Here, the CLaMS trajectories that are relevant for the Nabro volcano are shown together with the tropopause layer around June 21st, within a 3 days time frame. Both trajectories and tropopause are color-coded by altitude, though with different color scales to provide contrast.

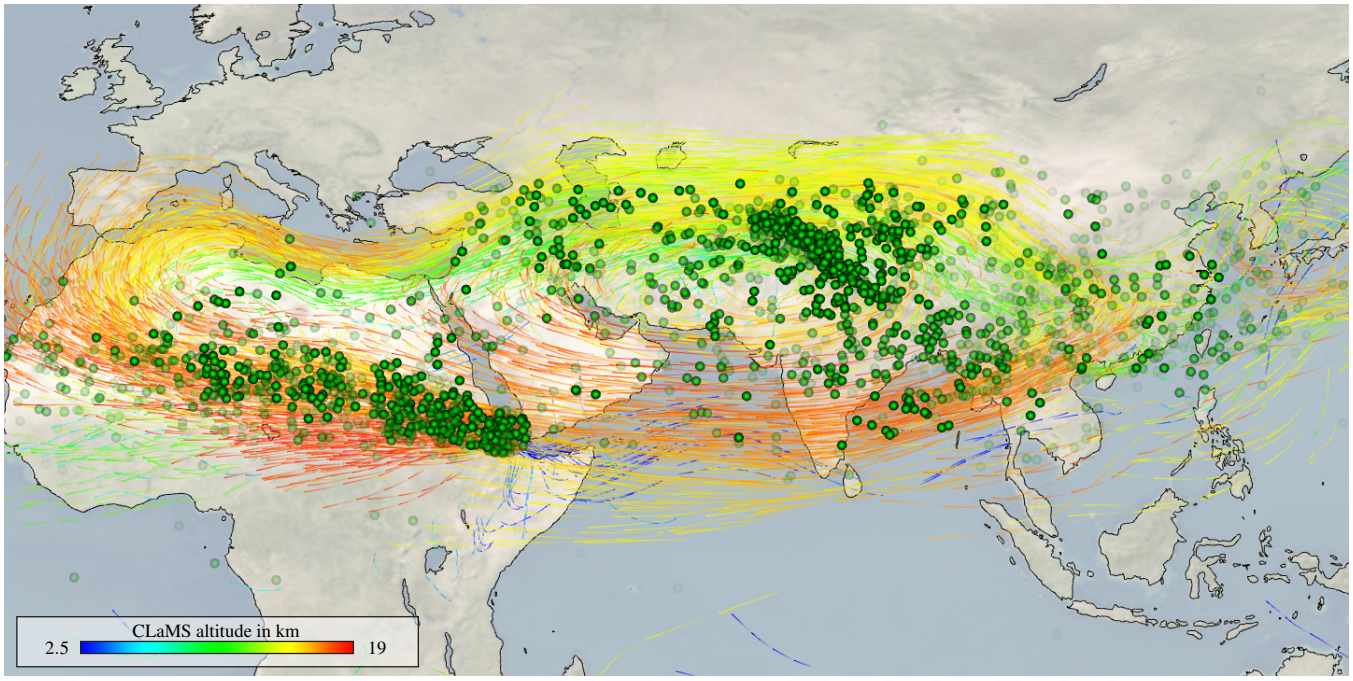

(a) Intersections of CLaMS trajectories with the tropopause.

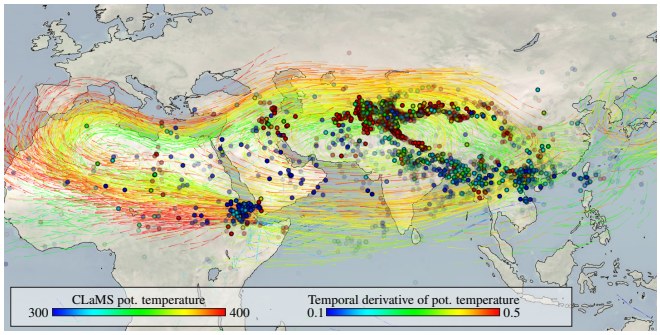

(b) Maximal change in potential temperature.

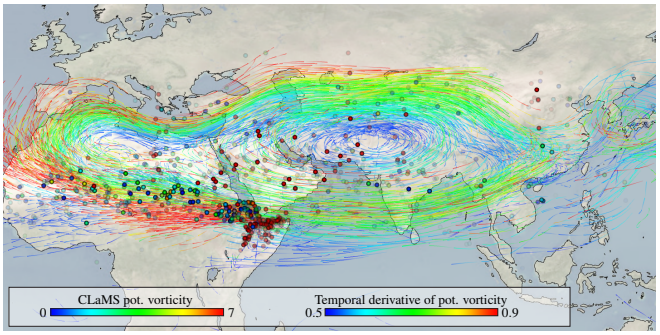

(c) Maximal change in potential vorticity.

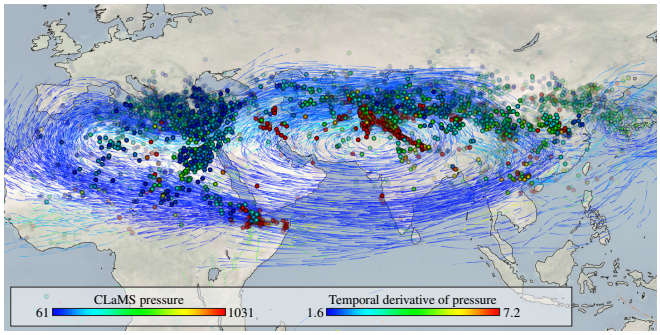

(d) Maximal change in pressure.

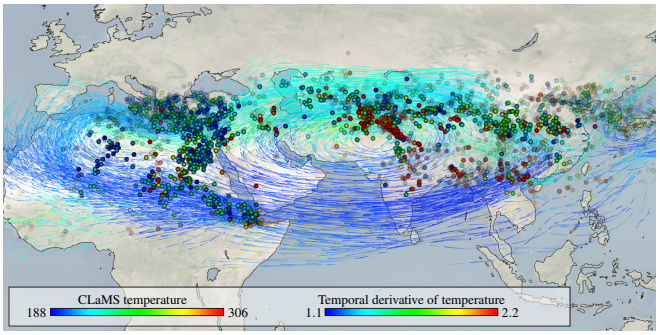

(e) Maximal change in temperature.

Figure 11: There are a number of different indicators that suggest a transition of a particle into the stratosphere. In this image, a few of them are shown, plotted as points for the entire time sequence. Points in (a) are intersections of CLaMS trajectories with the lower tropopause geometry layer. The accompanying CLaMS trajectories are color-coded by altitude. A point in (b) to (e) represents the global maximum of the derivative of a certain scalar attribute of a line. Derivatives are with respect to time in Julian hours. The magnitude of the respective derivative is encoded by the point color with the AIRS SO_2 index mapped to opacity ($[0.5, 1] \rightarrow [0, 1]$). The underlying scalar attribute of the line is color-coded on the CLaMS trajectories for reference. CLaMS trajectories are only shown for a time window of 36 hours centered around June 26th in order to reduce clutter.